Fluctuation and Noise Letters

The Stochastic Origin of Random Telegraph Noise

Francesco Maria Puglisi
Dipartimento di Ingegneria "Enzo Ferrari", University of Modena and Reggio Emilia, Via P. Vivarelli 10/1 Modena, 41125, Italy
francescomaria.puglisi@unimore.it

Received Day Month Year
Revised Day Month Year
Accepted Day Month Year
Published Day Month Year

Communicated by

Lately, Random Telegraph Noise (RTN) has been deemed, via specific mathematical metrics, to be possibly deterministic-chaotic rather than stochastic, with severe implications for applications that leverage on the RTN stochastic nature. Yet, this was claimed by analyzing a limited number of RTN traces. Here we analyze several RTN traces measured in different devices and conditions, mathematically generated traces, and traces resulting from advanced simulations of RTN in MIM structures. It is shown that the mathematical metrics employed to reveal the deterministic-chaotic nature of RTN are not robust enough to support that claim. Complex RTN is likely to result from inherently stochastic processes embedded in a deterministic multi-body system which could show stochastic chaos, but hardly any determinism.

Keywords: Random Telegraph Noise; stochastic; deterministic; chaotic; RRAM; FinFET.

1. Introduction

Random Telegraph Noise (RTN) is well known to be one of the most degrading effects in modern electron devices. Especially as devices scale closer to the atomic size, its effects are forecasted to be increasingly severe, ultimately limiting the reliability of devices, circuits, and systems. Therefore, a complete understanding of the physical mechanisms behind RTN is essential. Although it is well established that RTN results from charge trapping and de-trapping into and out of defects, most often in dielectrics or space charge regions of electron devices, some aspects remain ambiguous and need a more refined comprehension. Lately, a key aspect of RTN, which was previously given for granted, i.e., its inherent randomness, was challenged by a few contributions in the literature. Specifically, in RTN measured in MOSFETs [1] and RRAMs [2] has been suggested to be not stochastic, as previously thought. In fact, by using specific metrics such as the correlation dimension in the context of the Grassberger-Procaccia method and the Lyapunov spectrum, it was proposed that complex RTN could be originating from a deterministic-chaotic system rather than from stochastic one [1-2]. If confirmed, this would have very serious consequences for emerging applications in which RTN's alleged true

randomness is harnessed and exploited as entropy source, e.g., true random number generators [4-8]. Yet, such a bold claim was derived by analyzing a very limited number of measured or mathematically generated RTN traces, undermining its strength. Here we analyze several RTN traces measured in different devices and conditions, mathematically generated RTN traces, and complex RTN resulting from advanced kinetic Monte-Carlo simulations of charge transport and trapping in MIM structures in order to possibly shed light on the dynamic nature of the systems underlying the observed RTN time-series. Results show that it is highly likely that the mathematical tools mentioned above and previously employed to claim the possible deterministic chaotic nature of RTN are not robust enough to substantiate that bold claim. A self-consistent physical picture of RTN suggests its random nature, which might however be coexistent with chaotic (yet non-deterministic) features emerging from electrostatic interactions between defects.

2. Devices, Experiments, and Simulations

In the following, we report the details of *i*) the devices on which RTN was measured (and the associated measurement conditions); *ii*) the devices in which RTN was simulated (and the details of the employed simulation platform); *iii*) the mathematically generated RTN time-series.

2.1. *Experiments*

RTN traces were measured in 28-nm bulk n-FinFETs with a TiN/1.8nm HfO_2/0.6nm SiO_x/Si structure, each having two parallel 10nm-wide, 30nm-high, and 70nm-long fins (sketched in Fig. 1a).

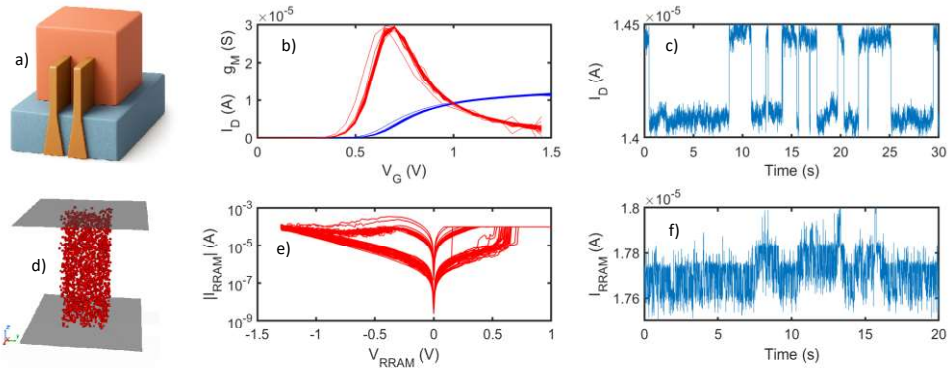

Fig. 1. a) Sketch of a bulk FinFET with two fins; b) I_D-V_G (blue lines) and corresponding g_M-V_G (red curves) of FinFET devices measured at T=300K and V_D=0.1V; c) I_D vs. time recorded on a FinFET device with V_G=0.7V and V_D=0.5V; d) Sketch of a RRAM device with the conductive filament in evidence; e) I_{RRAM}-V_{RRAM} (red lines) measured during multiple set and reset operations. For this specific device, the set operation is executed under a current compliance of 100μA; f) I_{RRAM} vs. time recorded on a RRAM device in high resistive state (achieved with a reset operation at V_{RESET}=-0.9V) with V_{READ}=30mV, T=343K.

A Keithley 4200-SCS, providing a current noise floor of about 100pA RMS, was employed to perform static I_D-V_G and transient I_D-time (RTN) measurements. First, the devices functionality was tested with I_D-V_G curves, as shown in Fig. 1b. Then, FinFETs at T = 30°C were biased at V_{GS} = 0.7V or 0.72V and V_{DS} = 0.5V, while the drain current was sampled every 7ms for 30s to record RTN traces. An example of such a recorded RTN trace is given in Fig. 1c. Then, the devices were driven in high resistive state using DC sweeps down to V_{RESET} = -0.9V, -1.0V or -1.1V and were then read to record RTN at T ranging from 30°C to 70°C under a DC voltage V_{READ} ranging from 10mV to 50mV, with a sampling time of 2ms or 6ms for a total measurement time of 20s or 60s, respectively. An example of a recorded RTN trace is given in Fig. 1f.

2.2. *Simulations*

We simulated RTN in a Metal-Insulator-Metal (MIM) structure having TiN electrodes and a 4 nm thick HfO_2 (EOT ≈ 0.74 nm) layer (see Fig. 2b and 2c). By using Ginestra® device simulation software [9], kinetic Monte-Carlo (kMC) 3D simulations were run to properly consider charge trapping dynamics and correctly simulate RTN [10]. In all simulations, we included all the key charge transport mechanisms occurring in a dielectric, see Fig. 2a.

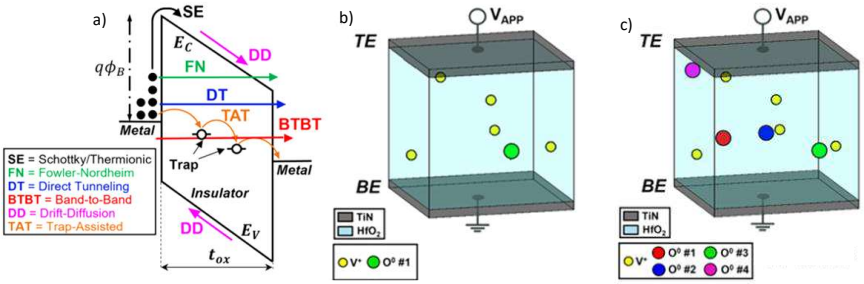

Fig. 2. a) The main conduction mechanisms occurring in dielectrics and considered in this work; b-c) Sketch of a simulated MIM cell with five V^+ defects and b) a single O^0 defect or c) four O^0 defects.

Specifically, we included Schottky/thermionic emission (SE), direct tunneling (DT), Fowler-Nordheim tunneling (FN), band-to-band tunneling (BTBT), drift/diffusion in conduction and valence band (DD), and non-radiative multi-phonon trap-assisted (TAT) tunneling, including all possible charge transitions, i.e., capture/emission from/to top (TE) and bottom (BE) electrode, conduction (CB) and valence (VB) band, other defects (trap-to-trap contribution is considered). For a given defect distribution, the TAT model in Ginestra® [9,11-12] calculates the current in the dielectric considering the process reported in detail in [12]. In the framework of the TAT model, two key parameters define charge trapping dynamics at defects, i.e., the relaxation energy (E_{REL}), that describes how localized defect states couple to phonons, and the thermal ionization energy (E_{TH}), that is the energy required to promote an electron from the defect to the conduction band. The values of E_{REL} and E_{TH} are typically calculated for each defect species and charge state transition via DFT

simulations [13,14]. In our simulations (Fig. 2), we include oxygen vacancies (V^+, i.e., positively charged if empty and neutral upon e^- trapping) and oxygen ions (O^0, i.e., neutral if empty and negatively charged upon e^- trapping). Indeed, V^+ defects are the most involved in trap-assisted charge transport [11,12], while O^0 play a crucial role in resistive switching and in determining RTN [10,15]. We employ E_{REL} = 1.2 eV and E_{TH} = 2.2 ± 0.5 eV for V^+, while E_{REL} = 2.65 eV and E_{TH} = 2.3 ± 0.5 eV for O^0, consistent with DFT [13,14] and multi-scale simulations [11-12,15]. Since capture and emission time constants scale exponentially with E_{REL}, V^+ are typically seen as *fast traps* given their lower E_{REL} (compared to O^0). Thus, they can conduct a substantial current in the dielectric. Conversely, O^0 do not significantly contribute to charge transport. Most importantly, the full 3D Poisson equation is solved including the trapped charge term to account for electrostatic interactions in the dielectric due to the trapped charge [16-18] and to consider its effect on the local 3D potential profile and on the tunneling barriers for SE, DT, BTBT, and TAT. Indeed, RTN primarily emerges from an O^0-induced modulation of the TAT leakage current driven by V^+. In fact, when an ion captures an electron, the trapped charge alters the local potential at the V^+ defects in its vicinity. This reflects in a change in the V^+ capture and emission times, thus in the TAT current they drive. Upon the emission of charge from the ion, the previous value of the local potential at the V^+ defects nearby is restored, along with the TAT current value. This dynamic occurs for each O^0 (which also interact likewise with nearby O^0 defects, not only with V^+) potentially resulting in a complex time-dependent multi-body problem which produces the observed RTN [16-18]. In order to shed light on whether complex electrostatics interactions between O^0 defects (from which complex RTN has been shown to emerge [16-18]) may be involved in the alleged chaotic behavior observed in some measured RTN time-series [1-2], we simulated two different devices, shown in Fig. 2b and 2c, respectively. In device #1 (in Fig. 2b) five V^+ defects (responsible for the leakage current) and a single O^0 defect (giving RTN) are present. Conversely, device #2 (in Fig. 2c) shows four O^0 defects, some of which close enough to one another to potentially interact electrostatically, giving rise to a complex system which may indeed show high sensitivity to initial conditions.

2.3. *Synthesized Random Telegraph Noise*

In order to further examine the reliability of the data analysis procedures typically employed to ascertain the possible deterministic character of RTN (explained in the following section) we also mathematically synthesized four time-series. The first, shown in Fig. 3a, has fixed dwell times, both equal to 100 (in arbitrary time units) and has no Additive White Gaussian Noise (AWGN), resulting in a non-chaotic, fully deterministic signal (the absence of AWGN is indicated in Fig. 3a as σ/μ = 0%). The second is identical to the first but includes a quite weak AWGN, with σ/μ = 0.3%. Its plot would be essentially indistinguishable from the one in Fig. 3a, except by largely zooming in (as exemplified in the inset in Fig. 3a). Notably, this signal is supposedly deterministic and non-chaotic by design, but includes a weak noise component that in fact is intrinsically associated with a deterministic chaotic system. Indeed, AWGN is generated in software via a Pseudo-

Random Number Generator (PRNG), i.e., a deterministic chaotic system. In the third signal, shown in Fig. 3b, the AWGN is quite stronger, with $\sigma/\mu = 30\%$. Finally, the fourth signal, shown in Fig. 3c, has exponentially distributed dwell times, consistent with the Markov property of RTN [19]. The average capture and emission times are both equal to 100 (in arbitrary time units) and AWGN with $\sigma/\mu = 30\%$ is included. In this case, the PRNG is used both to synthesize the AWGN and to draw samples from the exponential distributions of capture and emission times. The signal is thus expected to be deterministic chaotic by design. This latter consideration is quite important, since in the literature a synthesized RTN signal akin to the one in Fig. 3c was analyzed using the methodologies outlined in the following section, and the results suggested a non-chaotic nature of the signal [1]. This finding was used to suggest that a mathematically synthesized RTN signal could not display any chaotic behavior since it was deemed to originate from simple mathematical formulations that do not account for interactions between defects, which might be at the origin of the chaotic behavior. Nevertheless, such signals should in fact show a chaotic behavior, since PRNGs (that inherently produce chaotic deterministic time-series) are employed to generate both the RTN signal and the AWGN component.

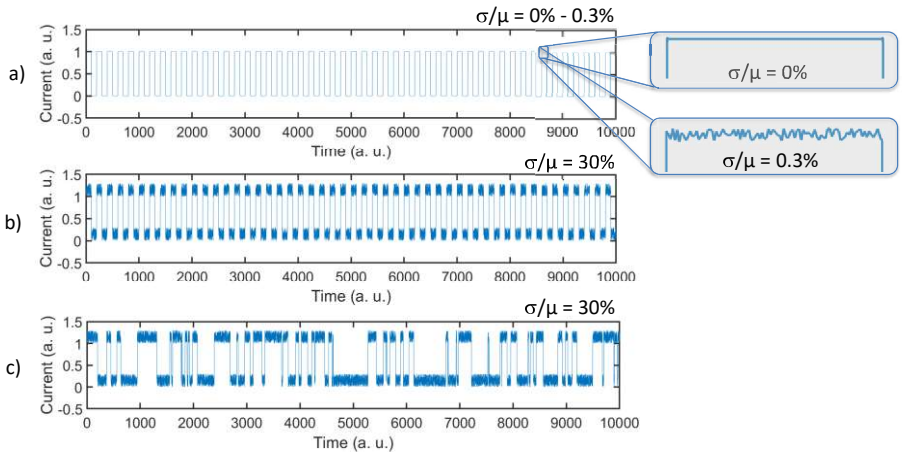

Fig. 3. Mathematically synthesized RTN time series with a) fixed dwell times both equal to 100 (in arbitrary time units) and no ($\sigma/\mu = 0\%$) or very weak ($\sigma/\mu = 0.3\%$) AWGN (the insets show the zoom-in detail of the two different time series); b) fixed dwell times both equal to 100 (in arbitrary time units) and stronger ($\sigma/\mu = 30\%$) AWGN; c) exponentially distributed dwell times with both average values equal to 100 (in arbitrary time units) and stronger ($\sigma/\mu = 30\%$) AWGN.

3. Mathematical Tools

In order to evaluate whether the system responsible for the generation of an observed noisy time-series is deterministic (chaotic) or stochastic, nonlinear dynamics tools are frequently employed. The two most significant methodologies, that are also the ones employed in this paper, are the Grassberger–Procaccia method [20] and the calculation of Lyapunov exponents [21]. In some contributions [2] additional approaches such as the surrogate data

method, are used besides the ones above to further reinforce the findings obtained with the latter. Nevertheless, here we will focus on the two most relevant and widespread techniques. In the remainder of the section, these two methodologies are briefly described and some key considerations are drawn.

3.1. *Grassberger-Procaccia Method*

Grassberger and Procaccia set forth [20] a method for evaluating the presence of deterministic chaos in a system based on the evaluation of the correlation and minimum embedding dimensions. It requires mapping a measured time-series to a topologically equivalent phase space. According to the Takens theorem [22], the topologically equivalent attractor in a higher-dimensional phase space can be reconstructed from an observed time-series Y [1-2,22]. To project the latter in an m-dimensional phase space, each point $Y(t_i)$ of the time-series is associated with a point X_i in the m-dimensional phase space by a state vector, built using the time-delay method, see eq. (1).

$$X_i = \{Y(t_i), Y(t_i + \tau), Y(t_i + 2\tau), \dots, Y(t_i + (m-1)\tau)\} \quad (1)$$

In eq. (1), m is the embedding dimension and τ is the time delay, which must be carefully estimated for proper embedding and phase space reconstruction. The time delay τ is usually estimated as the first minimum of the auto correlation function of the time-series, or using the average mutual information (AMI) method. The latter consists in calculating the AMI between the time-series and its delayed version (using a time delay t) for different values of t, i.e., AMI(t). Then, the time delay τ is estimated as the t at which the first minimum of AMI(t) occurs. The minimum embedding dimension can be calculated by means of the False Nearest Neighbor method. The Grassberger–Procaccia method uses the state vector in the m-dimensional phase space to first calculate the correlation integrals $C_m(r)$ as per eq. (2) [1-2,20].

$$C_m(r) = \lim_{N\to\infty} \frac{1}{N^2} \sum_{\substack{i,j=1 \\ i\neq j}}^{N} \Theta\left[r - \sqrt{\sum_{k=1}^{m} \left|X_{j+k} - X_{i+k}\right|^2}\right] \quad (2)$$

where N is the number of points of the reconstructed attractor, r is the radius of similarity, m the embedding dimensions, and Θ is the step (Heaviside) function. In essence, the correlation integral is an estimate of the mean probability that the states at two different times are closer than r. For a given value of m, C_m is calculated for different r, and the slope of the linear part of $C_m(r)$, i.e., the correlation dimension ν_m, is estimated. This calculation is repeated for different values of m, building a ν_m vs. m plot. Grassberger-Procaccia posit that in the case of noise-perturbed systems ν_m increases with m, while for deterministic chaos perturbed by weak noise ν_m will increase with m to a point and then saturate. Thus, we will use the presence of a saturating trend in the ν_m vs. m plot as a metric to possibly determine whether the system underlying the observed time-series is stochastic or rather showing deterministic chaos perturbed by weak noise. However, it is quite important to

underline that examples contradicting this have been reported [23-24], indicating that this metric cannot be always fully trusted.

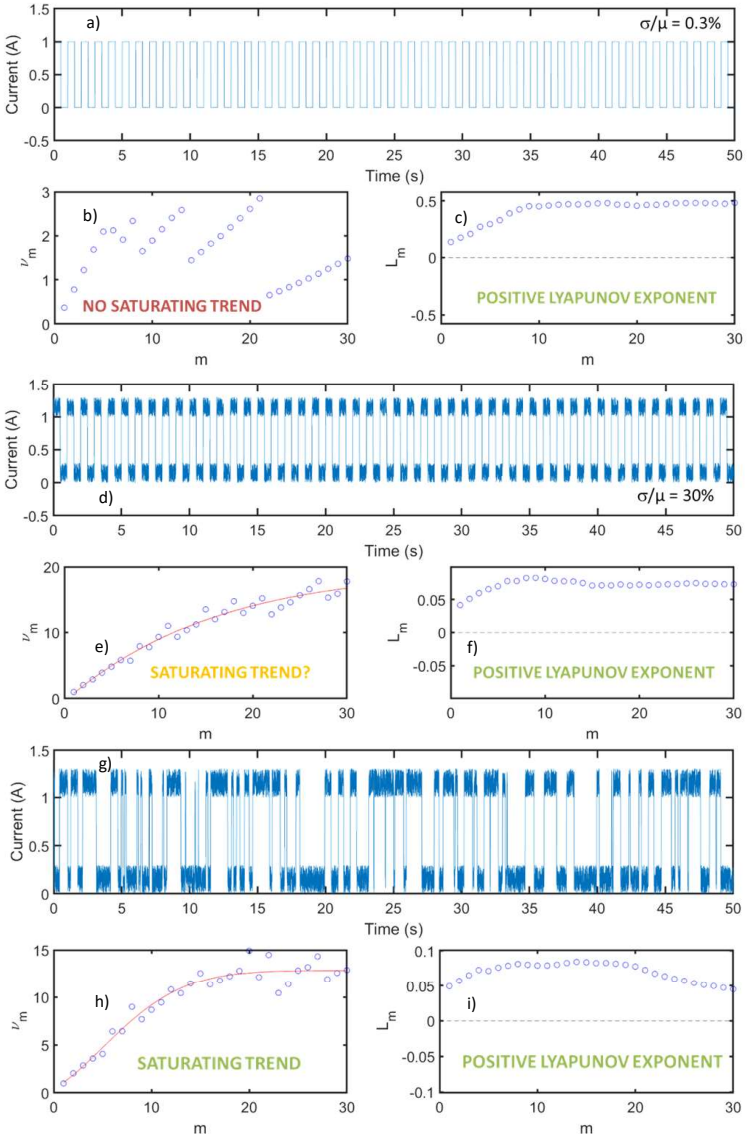

Fig. 4. The mathematically synthesized RTN time series a) in Fig. 3a with very weak (σ/μ = 0.3%) AWGN, d) in Fig. 3b, and g) in Fig. 3c, together with the associated ν_m vs. m plot (respectively in panels b, e, h) and L_m vs. m plot (respectively in panels c, f, i). In the ν_m vs. m plots a fitting trend line is reported as a guide to the eye.

3.2. *Lyapunov Exponents*

Lyapunov exponents are quantities that evaluate the rate of separation of infinitesimally close trajectories, thus giving a measure of sensitivity to initial conditions of a system. As the rate of separation can be different for different directions in the phase space, the number of Lyapunov exponents equals the dimensionality of the phase space, m. The largest (or maximal) Lyapunov exponent for a given value of m, L_m, is of specific interest, as a positive L_m is usually taken as an indication that the system is chaotic. Therefore, we will use the sign of L_m at different m as a metric to possibly determine whether the system underlying the observed time-series is stochastic or rather deterministic chaotic. Nevertheless, it is important to underline that the presence of positive Lyapunov exponents is a mere clue for deterministic chaos and not a direct proof. Indeed, in some cases stochastic systems can show similar features to those of deterministic chaotic systems [25]. This indicates that this metric cannot be always fully trusted.

4. Results

The synthesized, measured, and simulated RTN traces are now evaluated using the metrics described in Section 3 to possibly draw conclusions about the dynamic nature of the system underpinning RTN. Initially, we evaluated the four synthesized signals discussed in Section 2.3. The first signal is fully deterministic by design and indeed shows $\nu_m = L_m = 0$ for all m values, as expected (not shown). Interestingly, the second signal, which includes a quite weak PRNG-generated AWGN with $\sigma/\mu = 0.3\%$, shows a positive L_m for all m values, which points at the presence of chaos, while the ν_m vs. m plot shows no saturating trend, suggesting the absence of chaos. The analysis, summarized in Fig. 4a-b-c, suggests that L_m, unlike ν_m, might be a metric quite sensitive to the presence of PRNG-generated components, even when they are very weak. The third signal, which includes a stronger PRNG-generated AWGN with $\sigma/\mu = 30\%$, shows again a positive L_m for all m values, and the ν_m vs. m plot starts showing a possibly saturating trend, which hints at chaos. In this case both metrics are picking up the chaotic features of the PRNG-generated AWGN. Finally, the fourth signal, which features (PRNG-)distributed capture and emission times for the RTN as well as a PRNG-generated AWGN with $\sigma/\mu = 30\%$, shows positive L_m for all m values and a clear saturated ν_m vs. m plot, which might be interpreted as a strong indication of chaos. However, it is quite clear that here chaos emerges from the use of PRNGs. These findings suggest that synthesized RTN signals should not be used as a benchmark to validate the reliability of these (and similar) metrics as they are inherently affected by chaotic components. Furthermore, the contrasting results in the literature [1], in which a synthesized RTN signal showed a non-saturated ν_m vs. m characteristics makes it even harder to full trust these metrics to possibly claim that RTN might be a deterministic chaotic phenomenon.

RTN signals measured in n-FinFETs all show a saturated ν_m vs. m curve and negative L_m, thus the metrics are in contrast. The results of the analysis on two devices measured at different V_G values are reported in Fig. 5. In the light of the results obtained on synthesized

RTN signal, one would be inclined to exclude the presence of chaos in these time-series, as given the negative L_m (since the latter has been shown to be more sensitive to the presence of chaotic components than ν_m). Nevertheless, also in this case the clashing metrics hinder the possibility of claiming a deterministic chaotic nature of RTN.

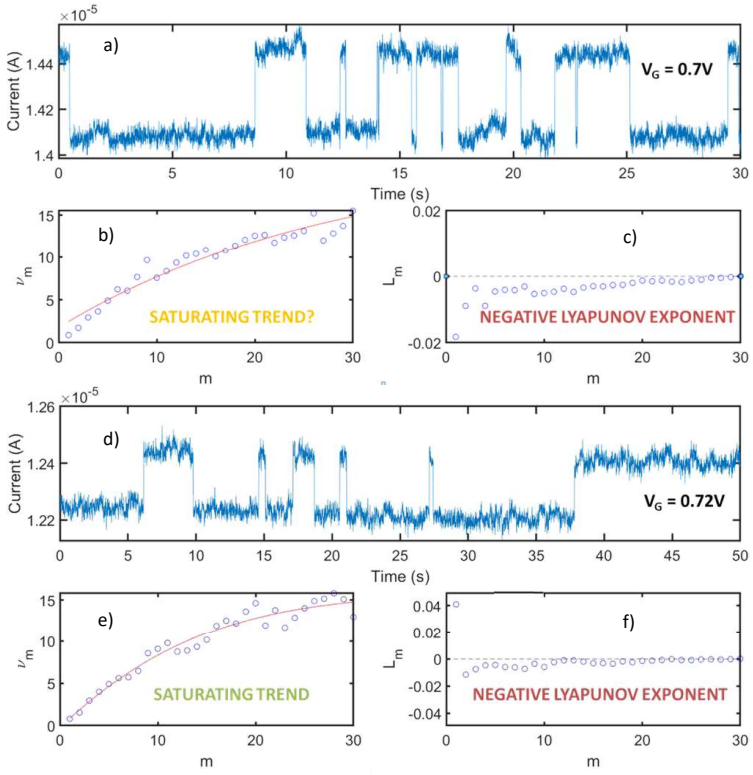

Fig. 5. RTN time series experimentally measured in FinFET devices at a) $V_G = 0.70$V and d) $V_G = 0.72$V, together with the associated ν_m vs. *m* plot (respectively in panels b and e) and L_m vs. *m* plot (respectively in panels c and f). In the ν_m vs. *m* plots a fitting trend line is reported as a guide to the eye.

RTN signals measured in RRAM devices always shows a saturated ν_m vs. *m* curve but L_m is found to be either positive or negative depending on the specific time-series, which is again inconclusive. The results of the analysis on two time-series acquired consecutively on the same device in the same resistive state and in the same conditions are reported in Fig. 6a-b-c and Fig. 6d-e-f, respectively. Interestingly, while the two RTN time-series are very similar to one another even at eye inspection (as one should expect since the two measurements were performed sequentially without altering the state of the device), the analysis of the first signal reveals a positive L_m while a negative L_m is found in the second, again suggesting that these metrics are hardly trustable to make claims about the dynamic nature of RTN. Finally, the analysis of the RTN time-series obtained by simulations on device #1 (in which just one O^0 defect is present) shows a non-saturated ν_m vs. *m* curve and

positive L_m, with metrics again in contrast, see Fig. 7a-b-c. Conversely, when multiple O^0 defects are present and sufficiently close to one another to influence each other's charge trapping dynamics (device #2), complex RTN emerges (Fig. 7d) that shows saturated ν_m vs. *m* curve and positive L_m, suggesting the presence of chaos (Fig. 7e-f).

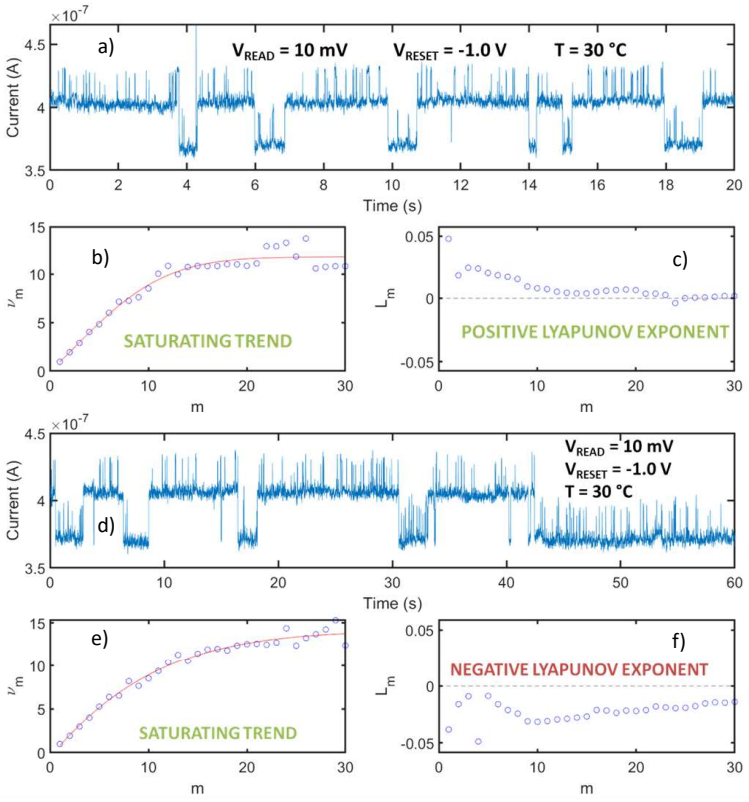

Fig. 6. RTN time series experimentally measured in RRAM devices in HRS (achieved with V_{RESET} = -1.0V) and sequentially acquired at V_{READ} = 10 mV and T = 30 °C using a sampling time of a) 2ms and b) 6m, together with the associated ν_m vs. *m* plot (respectively in panels b and e) and L_m vs. *m* plot (respectively in panels c and f). In the ν_m vs. *m* plots a fitting trend line is reported as a guide to the eye.

The overall picture that emerges from these results is that most probably these metrics are inadequate to make bold claims about the dynamic nature of RTN, which is in line with that both the presence of a saturated ν_m vs. *m* curve and/or of a positive L_m are hints for the presence of deterministic chaos and not proof of that. A sounder interpretation shall be based on the remark that, unlike what these methods tend to imply, chaos and randomness are not mutually exclusive (i.e., chaos is not necessarily deterministic) [26]. In fact, a system may concurrently be sensitively dependent upon initial conditions (chaotic) and randomly perturbed by noise (stochastic), which undermines any attempt to identify system dynamics as simply deterministic chaos or stochastic chaos. In the specific case of RTN, it is important to recall that there is unanimous consensus on the fact that the physical process

at its origin is always associated with tunneling (i.e., RTN results from tunneling events), that is a purely quantum, thus stochastic, phenomenon with no associated classical deterministic description. In this sense, the mathematical description of the physical system responsible for RTN as described in Section 2.2 can be classified as a stochastic since, while the tunneling *rates* are calculated with a deterministic approach, the actual instants of time at which tunneling events happen are random. However, as demonstrated in the literature and remarked in Section 2.2, electrostatic interactions between defects, if present, may result in a complex multi-body problem [16-18], likely to show high sensitivity to initial conditions (thus chaotic features), yet superposed to an inherent randomness for the above reasons.

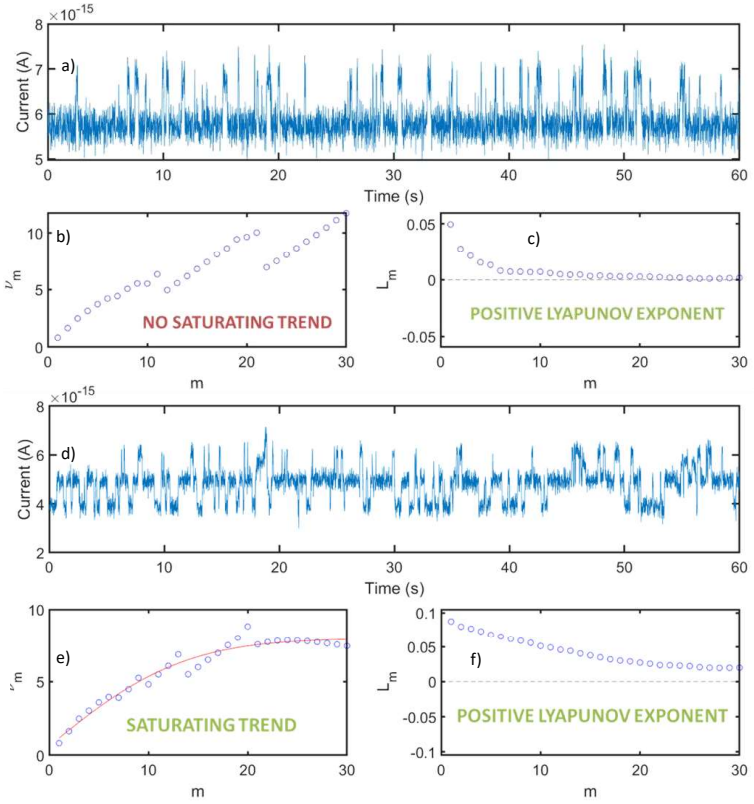

Fig. 7. RTN time series simulated measured in the MIM stacks in Fig. 2b and 2c (panels a and d, respectively), together with the associated ν_m vs. m plot (respectively in panels b and e) and L_m vs. m plot (respectively in panels c and f). In the ν_m vs. m plots a fitting trend line is reported as a guide to the eye.

In conclusion, due to its very physical nature, RTN is hardly a deterministic phenomenon and likely always maintains an inherent stochastic character. Nevertheless, it may or may not show chaotic features depending on the complexity and extent of electrostatic interactions between defects.

Acknowledgements

This study received funding from PNRR–M4C2INV1.5, NextGenerationEU - Avviso 3277/2021 - ECS_00000033 – ECOSISTER - Spoke 6 - CUP E93C22001100001.

ORCID

Francesco Maria Puglisi - https://orcid.org/0000-0001-6178-2614

References

[1] D. H. Tassis, S. G. Stavrinides, M. P. Hanias, C. G. Theodorou, G. Ghibaudo and C. A. Dimitriadis, "Chaotic Behavior of Random Telegraph Noise in Nanoscale UTBB FD-SOI MOSFETs," in IEEE Electron Device Letters, vol. 38, no. 4, pp. 517-520, April 2017, doi: 10.1109/LED.2017.2672783.

[2] S. G. Stavrinides, M. P. Hanias, M. B. Gonzalez, F. Campabadal, Y. Contoyiannis, S. M. Potirakis, M. M. Al Chawa, C. de Benito, R. Tetzlaff, R. Picos, L. O. Chua, "On the chaotic nature of random telegraph noise in unipolar RRAM memristor devices," in Chaos, Solitons & Fractals, Volume 160, 2022, 112224, ISSN 0960-0779, doi: 10.1016/j.chaos.2022.112224.

[4] M. Lanza et al., "Memristive technologies for data storage, computation, encryption, and radio-frequency communication." Science, 376, eabj9979(2022). doi: 10.1126/science.abj9979.

[5] X. Li, T. Zanotti, T. Wang, K. Zhu, F. M. Puglisi, M. Lanza, "Random Telegraph Noise in Metal-Oxide Memristors for True Random Number Generators: A Materials Study," Adv. Funct. Mater. 2021, 31, 2102172. doi: 10.1002/adfm.202102172.

[6] C. Wen, X. Li, T. Zanotti, F. M. Puglisi, Y. Shi, F. Saiz, A. Antidormi, S. Roche, W. Zheng, X. Liang, J. Hu, S. Duhm, J. B. Roldan, T. Wu, V. Chen, E. Pop, B. Garrido, K. Zhu, F. Hui, M. Lanza, "Advanced Data Encryption using 2D Materials," Adv. Mater. 2021, 33, 2100185. doi: 10.1002/adma.202100185.

[7] S. Pazos, W. Zheng, T. Zanotti, F. Aguirre, T. Becker, Y. Shen, K. Zhu, Y. Yuan, G. Wirth, F. M. Puglisi, J. B. Roldán, F. Palumbo, M. Lanza "Hardware implementation of a true random number generator integrating a hexagonal boron nitride memristor with a commercial microcontroller," Nanoscale, 2023,15, 2171-2180. doi: 10.1039/D2NR06222D.

[8] R. Serrano et al., "A Fully Digital True Random Number Generator With Entropy Source Based in Frequency Collapse," in IEEE Access, vol. 9, pp. 105748-105755, 2021, doi: 10.1109/ACCESS.2021.3099534.

[9] See https://www.appliedmaterials.com/il/en/semiconductor/ginestra-software.html for information about Applied Material's Ginestra simulation software.

[10] F. M. Puglisi, L. Larcher, A. Padovani and P. Pavan, "Characterization of anomalous Random Telegraph Noise in Resistive Random Access Memory," 2015 45th European Solid State Device Research Conference (ESSDERC), Graz, Austria, 2015, pp. 270-273, doi: 10.1109/ESSDERC.2015.7324766.

[11] L. Larcher, "Statistical simulation of leakage currents in MOS and flash memory devices with a new multiphonon trap-assisted tunneling model," in IEEE Transactions on Electron Devices, vol. 50, no. 5, pp. 1246-1253, May 2003, doi: 10.1109/TED.2003.813236.

[12] L. Vandelli, A. Padovani, L. Larcher, R. G. Southwick, W. B. Knowlton and G. Bersuker, "A Physical Model of the Temperature Dependence of the Current Through SiO2/HfO2 Stacks," in IEEE Transactions on Electron Devices, vol. 58, no. 9, pp. 2878-2887, Sept. 2011, doi: 10.1109/TED.2011.2158825.

[13] A. S. Foster, F. Lopez Gejo, A. L. Shluger, and R. M. Nieminen, “Vacancy and interstitial defects in hafnia,” Phys. Rev. B 65(17), 1741171–17411713 (2002). doi: https://doi.org/10.1103/PhysRevB.65.174117.

[14] N. Capron, P. Broqvist, and A. Pasquarello, “Migration of oxygen vacancy in HfO2 and across the HfO2/SiO2 interface: A first-principles investigation,” Appl. Phys. Lett. 91(19), 192905 (2007). doi: 10.1063/1.2807282.

[15] F. M. Puglisi, L. Larcher, A. Padovani and P. Pavan, "A Complete Statistical Investigation of RTN in HfO2-Based RRAM in High Resistive State," in IEEE Transactions on Electron Devices, vol. 62, no. 8, pp. 2606-2613, Aug. 2015, doi: 10.1109/TED.2015.2439812.

[16] S. Vecchi, P. Pavan and F. M. Puglisi, "The Relevance of Trapped Charge for Leakage and Random Telegraph Noise Phenomena," 2022 IEEE International Reliability Physics Symposium (IRPS), Dallas, TX, USA, 2022, pp. 1-6, doi: 10.1109/IRPS48227.2022.9764472.

[17] S. Vecchi, P. Pavan and F. M. Puglisi, "The Impact of Electrostatic Interactions Between Defects on the Characteristics of Random Telegraph Noise," in IEEE Transactions on Electron Devices, vol. 69, no. 12, pp. 6991-6998, Dec. 2022, doi: 10.1109/TED.2022.3213502.

[18] S. Vecchi, A. Padovani, P. Pavan and F. M. Puglisi, "From Accelerated to Operating Conditions: How Trapped Charge Impacts on TDDB in SiO_2 and HfO_2 Stacks," in IEEE Transactions on Device and Materials Reliability, vol. 24, no. 2, pp. 194-202, June 2024, doi: 10.1109/TDMR.2024.3384056.

[19] C. T. da Silveira, T. Exenberger Becker, P. A. Böckmann Alves and G. Inácio Wirth, "Implementation and Comparison of Algorithms for the extraction of RTN Parameters," 2021 35th Symposium on Microelectronics Technology and Devices (SBMicro), Campinas, Brazil, 2021, pp. 1-4, doi: 10.1109/SBMicro50945.2021.9585757.

[20] P. Grassberger, I. Procaccia, “Characterization of strange attractors,” Phys Rev Lett. 1983;50(5):346. doi: 10.1103/PhysRevLett.50.346.

[21] M. Sano, Y. Sawada, “Measurement of the lyapunov spectrum from a chaotic time series”, Phys Rev Lett. 1985;55(10):1082. doi: 10.1103/PhysRevLett.55.1082.

[22] F. Takens, “Detecting strange attractors in turbulence,” Dynamical systems and turbulence. Warwick 1980: Springer; 1981. p. 366–81. doi: 10.1007/BFb0091924.

[23] K. Fichthorn, E. Gulari, R. Ziff, “Noise-Induced Bistability in a Monte Carlo Surface-Reaction Model,” Phys. Rev. Lett., Vol.63, No.14, pp. 1527-1530, Oct. 1989. doi: 10.1103/PhysRevLett.63.1527.

[24] Z.-Y. Chen, “Noise-induced instability,” Phys. Rev. A 42, 5837. doi: 10.1103/PhysRevA.42.5837.

[25] A. Provenzale, L. A. Smith, R. Vio, G. Murante, “Distinguishing between low-dimensional dynamics and randomness in measured time series,” Physica D: Nonlinear Phenomena, Volume 58, Issues 1–4, 1992, Pages 31-49. doi: 10.1016/0167-2789(92)90100-2.

[26] M. Frey, Computational Stochastic Mechanics - Theory, Computational Methodology and Application, Elsevier Applied Science, London (1993).